Alfvén-Wave Propagation in Solid-State Plasmas. II. Bismuth§†

R. T. ISAACSON‡ AND G. A. WILLIAMS
Department of Physics, University of Utah, Salt Lake City, Utah 84112
(Received 13 August 1968)

Alfvén-wave propagation velocities in single-crystal bismuth have been studied for the frequency range 13 to 18 GHz, using an interference technique. Experimental mass densities were obtained for magnetic fields aligned along principal crystal axes. The variation of these mass densities for misalignment of the magnetic field and sample shape and size was also studied. The different values obtained by previous workers are shown to be due to minor sample misalignments. The number of carriers, n, and the mass components obtained are compared with values previously reported in the literature. The de Haas–Shubnikov periods are also measured from the transmission envelope of the microwaves. The best fit to the numerical results for the carrier masses and the number of carriers obtained in this work is $n=(3.00\pm0.15)\times10^{17}$ cm^{-3}, $m_1=0.005\pm0.0015$, $m_2=1.27\pm.007$, $m_3=0.031\pm0.004$, $m_4=0.157\pm0.008$, $M_1=0.064$, and $M_3=0.69$. These parameters are shown to be consistent with all of the Alfvén-wave mass densities.

I. INTRODUCTION

THE presence of a magnetic field allows the propagation of low-frequency electromagnetic waves in metals and semimetals.[1–3] If either electrons or holes are the majority carrier, the wave propagates in the helicon mode.[2,3] This is the case for metals such as sodium and potassium. If the material has equal numbers of holes and electrons, as in the group-V semimetals, the wave propagates in the Alfvén mode. Alfvén-wave propagation in bismuth has been investigated in several laboratories.[4–17]

This paper reports studies of Alfvén-wave velocities in bismuth designed to resolve the experimental discrepancies between work in various laboratories. In some cases disagreements of up to 50% exist between different investigators for certain items of data. We have investigated the transmission of Alfvén waves through thin disks of bismuth using the interference technique of Williams.[7] The phase velocity of Alfvén waves depends on the carrier mass density; therefore the experimental velocities can be used to determine mass densities and thus obtain information on the number of carriers and their effective masses. We have investigated the variation of Alfvén-wave velocities due to slight misalignments of the sample with respect to the external magnetic field.

Section II presents the theory of Alfvén waves for anisotropic masses and infinite relaxation times. Section III is a discussion of the experimental and sample orientation details. Section IV presents the results, and Sec. V is a discussion of the results using the nonparabolic, ellipsoidal model for the electron Fermi surface.

II. THEORY

The theory of wave propagation in anisotropic plasmas, such as solid-state plasmas, has been discussed by Buchsbaum,[1] and Allis, Buchsbaum, and Bers.[14] The velocity of propagation of a wave whose propagation vector is $\mathbf{k}$ is most easily discussed using the concept of the effective dielectric tensor $\boldsymbol{\epsilon}$. The wave which propagates must be a solution of the wave equation

$$\nabla\times\nabla\times\mathbf{E}-(\omega^2/c^2)\boldsymbol{\epsilon}\cdot\mathbf{E}=0. \tag{1}$$

If the solution is of the form

$$\mathbf{E}=\mathbf{E}_0e^{i(\mathbf{k}\cdot\mathbf{r}-\omega t)}, \tag{2}$$

the dispersion relationship which results is, for $\eta^2=k^2c^2/\omega^2$,

$$A\eta^4-B\eta^2+C=0; \tag{3}$$

$$\begin{aligned}A&=\epsilon_{xx}\sin^2\theta+2\epsilon_{xz}\cos\theta\sin\theta+\epsilon_{zz}\cos^2\theta,\\ B&=\epsilon_{xx}\epsilon_{zz}-\epsilon_{xz}^2+(\epsilon_{xx}\epsilon_{yy}+\epsilon_{xy}^2)\sin^2\theta\\ &\quad+2(\epsilon_{yy}\epsilon_{xz}-\epsilon_{xy}\epsilon_{yz})\sin\theta\cos\theta\\ &\quad+(\epsilon_{yy}\epsilon_{zz}+\epsilon_{yz}^2)\cos^2\theta,\\ C&=\det|\boldsymbol{\epsilon}|,\end{aligned} \tag{4}$$

§ This work was supported by the U. S. Air Force Office of Scientific Research under Grant No. AFOSR 901-65.

† Based on a thesis submitted by R. T. Isaacson to the University of Utah in partial fulfillment of the requirements for the degree of Doctor of Philosophy.

‡ NASA Predoctoral Fellow, 1964–1966.

[1] S. J. Buchsbaum and J. K. Galt, Phys. Fluids **4**, 1514 (1961).
[2] S. J. Buchsbaum, *Symposium on Plasma Effects in Solids, Paris, 1964* (Academic Press Inc., New York, 1965).
[3] R. Bowers, *Symposium on Plasma Effects in Solids, Paris, 1964* (Academic Press Inc., New York, 1965).
[4] J. Kirsch, Phys. Rev. **133**, A1390 (1964).
[5] M. S. Khaikin, V. S. Edel'man, and R. T. Mina, Zh. Eksperim. i Teor. Fiz. **44**, 2190 (1963) [English transl.: Soviet Phys.—JETP **17**, 1470 (1963)].
[6] M. S. Khaikin, La. Fal'kovskii, V. S. Edel'man, and R. T. Mina, Zh. Eksperim. i Teor. Fiz. **45**, 1704 (1964) [English transl.: Soviet Phys.—JETP **18**, 1167 (1964)].
[7] G. A. Williams, Phys. Rev. **139**, A771 (1965).
[8] G. A. Williams and G. E. Smith, IBM J. Res. Develop. **8**, 276 (1964).
[9] D. S. McLachlan, Phys. Rev. **147**, 368 (1966).
[10] B. W. Faughnan, J. Phys. Soc. Japan **20**, 574 (1965).
[11] D. J. Bartelink and W. A. Nordland, Phys. Rev. **152**, 556 (1966).
[12] W. L. Lupatkin and C. A. Nanney, Phys. Rev. Letters **20**, 212 (1968).
[13] D. L. Carter and J. C. Picard, Solid State Commun. **5**, 719 (1967).
[14] W. P. Allis, S. J. Buchsbaum, and A. Bers, *Waves in Anisotropic Plasmas* (The MIT Press, Cambridge, Mass., 1963).
[15] H. Kawamura, S. Nagata, T. Nakama, and S. Takano, Phys. Rev. Letters **15**, 111 (1965).
[16] M. S. Khaikin and V. S. Edel'man, Zh. Eksperim. i Teor. Fiz. **49**, 1695 (1966) [English transl.: Soviet Phys.—JETP **22**, 1159 (1966)].
[17] S. Nagata and H. Kawamura, J. Phys. Soc. Japan **24**, 480 (1968).

where $\boldsymbol{\epsilon}$ is the dielectric tensor, $\mathbf{H}$ is the static magnetic field which is taken along the z axis, $\mathbf{k}$ is the propagation vector of the wave and lies in the xz plane making an angle θ with $\mathbf{H}$. In general, there are two modes of propagation as seen from the solution of the dispersion relation,

$$\eta^2=[B\pm(B^2-4AC)^{1/2}]/2A\,. \tag{5}$$

For each mode of propagation there are two solutions corresponding to waves traveling in opposite directions. The details of these solutions can be found elsewhere.[14]

For $\mathbf{H}$ along a crystal axis in bismuth the dielectric tensor simplifies to the form

$$\epsilon=\begin{bmatrix}\epsilon_{\perp_1} & \epsilon_\times & 0\\ \epsilon_\times & \epsilon_{\perp_2} & 0\\ 0 & 0 & \epsilon_{\parallel}\end{bmatrix}. \tag{6}$$

For the magnetic field along a bisectrix direction in bismuth (axis 2) this is only approximately true. For the dielectric tensor in the form (6) and $\theta=\frac{1}{2}\pi$, we obtain for Eq. (3) the two solutions

$$k^2=\epsilon_{\parallel}\omega^2/c^2,\qquad k^2=\left(\epsilon_{\perp_1}+\frac{\epsilon_\times^2}{\epsilon_{\perp_2}}\right)\omega^2/c^2 \tag{7a}$$

and for $\epsilon_{\perp_1}=\epsilon_{\perp_2}$

$$\epsilon_\perp=\epsilon_l-\frac{\omega_p^2}{\omega^2-\omega_c^2}-\frac{\Omega_p}{\omega^2\Omega_c^2},$$

$$\epsilon_\times=j\frac{\omega_p^2}{\omega^2-\omega_c^2}\cdot\frac{\omega_c}{\omega}-j\frac{\Omega_p^2}{\omega^2-\Omega_c^2}\cdot\frac{\Omega_c}{\omega}, \tag{7b}$$

$$\epsilon_{\parallel}=\epsilon_l-\frac{\Omega_p^2}{\omega^2}-\frac{\omega_p^2}{\omega^2}.$$

Here ω is the experimental frequency, $\omega_c=eH/m_ec$ is the electron-cyclotron frequency, $\Omega_c=eH/m_hc$ is the hole-cyclotron frequency, $\omega_p^2=4\pi ne^2/m_e$ is the electron-plasma frequency, $\Omega_p^2=4\pi pe^2/m_h$ is the hole-plasma frequency, n and p are the number density of electrons and holes, respectively, and ϵ_l is the lattice dielectric constant.

The wave described by the first solution of Eq. (7a) does not propagate under the conditions of this experiment, which are $\omega\ll\omega_c$, $\omega\ll\Omega_c$, $\omega_c\ll\Omega_p$, and $\omega_c\ll\omega_p$. The second solution in Eq. (7a) reduces to

$$k^2=(\omega^2/c^2)[\epsilon_\perp-(\epsilon_\perp/\epsilon_x^2)]. \tag{8}$$

In Eq. (8) the first term describes the propagation of Alfvén waves[2,3,7] and the second term describes the propagation of helicon waves.[2,3] Unless $p-n$ is nearly zero the helicon term is dominant. For pure bismuth the helicon term is zero. For magnetic fields less than 100 kG the lattice dielectric constant is also negligible and Eq. (8) becomes

$$k^2=(\omega^2/c^2)[(4\pi m_0c^2)f(nm_e^*+pm_h^*)/H^2]. \tag{9}$$

Here m_0 is the free-electron mass and $f(nm_e^*+pm_h^*)$ is the mass density term which depends on the crystal orientation with respect to the static magnetic field and the microwavelectric field. The theoretical expressions for $f(nm_e^*+pm_h^*)$ are given in Table V for various orientations of $\mathbf{H}$ and $\mathbf{E}$ with respect to the principal crystal axes.

The model of the bismuth Fermi surface used to interpret the experimental results consists of three electron ellipsoids and one hole ellipsoid. For one electron ellipsoid the Fermi surface is given by

$$E_F(1+E_F/E_G)=(\hbar^2/2m_0)(k_x^2/\alpha_1+k_y^2/\alpha_2+k_z^2/\alpha_3+2k_yk_z/\alpha_4), \tag{10}$$

where the α's are components of the inverse mass tensor $\mathbf{m}$:

$$\mathbf{m}=\begin{bmatrix}m_1 & 0 & 0\\ 0 & m_2 & m_4\\ 0 & m_4 & m_3\end{bmatrix},\quad \mathbf{m}^{-1}=\begin{bmatrix}\alpha_1 & 0 & 0\\ 0 & \alpha_2 & \alpha_4\\ 0 & \alpha_4 & \alpha_3\end{bmatrix}. \tag{11}$$

The other two electron ellipsoids are obtained by $\pm120°$ rotations about the z axis. The hole ellipsoid is given by

$$(E_0-E_F)=(\hbar^2/2m_0)(k_x^2/\beta_1+k_y^2/\beta_2+k_z^2/\beta_3), \tag{12}$$

where the β's are components of the hole inverse mass tensor:

$$\mathbf{M}=\begin{bmatrix}M_1 & 0 & 0\\ 0 & M_2 & 0\\ 0 & 0 & M_3\end{bmatrix},\quad \mathbf{M}^{-1}=\begin{bmatrix}\beta_1 & 0 & 0\\ 0 & \beta_2 & 0\\ 0 & 0 & \beta_3\end{bmatrix}. \tag{13}$$

E_F is the Fermi energy, E_g is the gap between the conduction band and filled valence band, and E_0 is the overlap energy. All other symbols have their usual meaning. Experimental evidence indicates that any nonellipsoidal shape of the Fermi surface is slight.[16,18–21] There is some evidence for a nonquadratic dependence of the hole-energy surface.[22,23] The Alfvén-wave velocities and mass densities do not depend on the exact energy dependence of the masses, since the mass-density expression is dependent only on the ellipsoidal character of the Fermi surface and the mass components at the Fermi surface.

III. EXPERIMENTAL

Figure 1 shows the sample holder for the Alfvén-wave transmission experiments. The magnetic field in these experiments was always parallel to the sample surface

[18] R. N. Bhargava, Phys. Rev. **156**, 785 (1967).
[19] N. B. Brandt, T. F. Dogolenko, and N. N. Stupuchenko, Zh. Eksperim. i Teor. Fiz. **45**, 1319 (1964) [English transl.: Soviet Phys.—JETP **18**, 908 (1964)].
[20] V. S. Edel'man and M. S. Khaikin, Zh. Eksperim. i Teor. Fiz. **49**, 107 (1965) [English transl.: Soviet Phys.—JETP **22**, 77 (1966)].
[21] A. P. Korolyuk, Zh. Eksperim. i Teor. Fiz. **49**, 1099 (1966) [English transl.: Soviet Phys.—JETP **22**, 701 (1966)].
[22] G. A. Antcliffe and R. T. Bate, Phys. Rev. **160**, 531 (1967).
[23] R. T. Bate and N. G. Einspruch, Phys. Rev. **153**, 796 (1967).

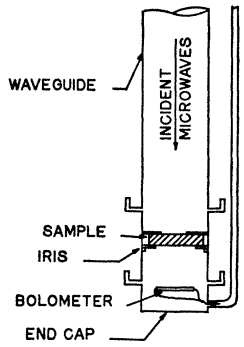

FIG. 1. Experimental sample holder.

and perpendicular to the direction of microwave propagation. The microwave radiation was linearly polarized and incident from above. The frequency range used was from 13 to 18 GHz. The sample thickness ranged from 1 to 9 mm. With the sample geometry as shown in Fig. 1, the transmitted wave intensity exhibited a series of maxima and minima, as seen in Fig. 2. The maxima in Fig. 2 are the fringes of the interference pattern. These interference fringes result from Fabry-Perot–type interference within the sample, or from interference between the transmitted signal and a signal that "leaked" around the sample. The Fabry-Perot type of pattern produces twice as many fringes as the leakage pattern.[7,8] The Fabry-Perot condition for intensity maximum requires an integral number of half-wavelengths of the microwaves in a sample thickness. The leakage condition for an intensity maximum requires an integral number of whole wavelength in the sample. At sufficiently high fields the Fabry-Perot pattern dominates the leakage pattern. What exactly is a "sufficiently high" magnetic field depends upon how well the "leakage" path is blocked. In these experiments all fringe patterns were of the leakage type. The intensity maxima are given by

$$\lambda_0 N = d\epsilon^{1/2} = dkc/\omega, \qquad (14)$$

where d is the sample thickness, λ_0 is the free-space wavelength of the microwave radiation, and N is the fringe index. The lowest value of N is assigned to the intensity maxima at largest magnetic field. Using Eq. (9) in Eq. (14), we obtain

$$N = (d/\lambda_0)[4\pi m_0 c^2 f(nm_e^* + pm_h^*)/H^2]^{1/2}. \qquad (15)$$

A plot of N versus $1/H$ gives a straight line whose slope is proportional to $f(nm_e^* + pm_h^*)$. Since we are interested only in the slope, the absolute value of N is not required. Any value can be assigned to the highest field maximum. The remaining maxima are numbered in increasing sequence, corresponding to the fact that each fringe or maximum represents an additional full wavelength thickness for the sample.

In Fig. 1 the top iris is machined to be perpendicular to the axis of the sample holder. The sample was mounted from the bottom and held by a removable iris and a retaining ring. The end cap containing the bolometer was soldered on with Wood's metal. Originally the end cap contained a movable plunger to make a tuned cavity. This scheme was discarded since tuning was difficult. The present arrangement gave large detected signal amplitudes and required no tuning. The bolometer has been described by Williams.[7,8] It measures microwave power. The microwave klystron's reflector voltage was modulated at a few cycles per sec. This caused the bolometer signal to be modulated at the same frequency. The bolometer signal was detected by a Princeton Applied Research lock-in amplifier Model JB-5 and the output was fed to a Hewlett-Packard Mosely X-Y recorder. The magnetic field was produced by a Varian Associates 15-in. magnet.

Samples were grown from Cominco bismuth of 99.9999% purity by a Bridgman technique and cut on a Servomet spark cutter. The final orientation was made by mounting the crystal in a jig that could be placed in a tool for etching the surface without removing the sample from the jig. The jig could also be placed in a

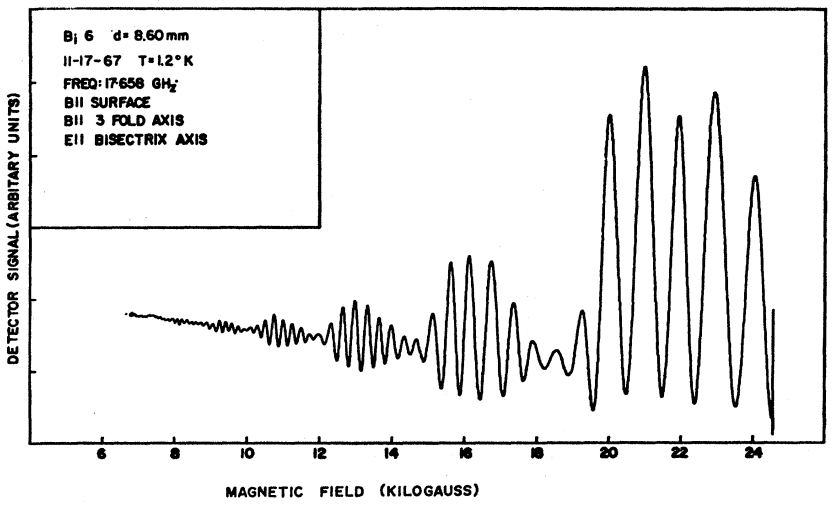

FIG. 2. Sample of experimental data. The modulation in amplitude is due to de Haas–Shubnikov oscillations in the attenuation of the Alfvén waves.

back-reflection Laue camera for checking the orientation of the crystal. All samples had one principal crystal axis perpendicular to the sample surface. Alignment of one axis perpendicular to the sample surface was better than 1°.

The alignment of the top iris was checked by putting a front surfaced mirror in place of the sample. The experimental probe was 51 in. long. The diameter of the probe was 0.825 in. and the iris diameter was 0.25 in. By looking down the tube it was possible to see the reflection of the pupil of the eye. This indicated that the mirror was perpendicular to the tube axis to within 0.3 of a deg; therefore, the sample would be perpendicular to this accuracy also. The experimental probe was only $\frac{1}{16}$ in. smaller than the inner diameter of the helium Dewar. This would allow an additional error of 0.1 of a degree, at most, in perpendicularity of the sample. The outside of the helium Dewar was aligned parallel to the pole faces of the magnet to about 0.2 of a degree. The cumulative effect of these orientation errors was that the plane of the top surface of the sample was believed to be parallel to the direction of the magnetic field to within 1°.

If there were an error in the perpendicularity of the experimental probe with respect to the magnet field, the magnetic field would not be exactly parallel to the sample surface. To check this, a series of data runs were made as the magnetic field was rotated. The sample holder was left in the same orientation with respect to the external field, but the sample was rotated with respect to the sample holder. A new series of runs as a function of angle would then produce slightly different values of $f(nm_e^*+pm_h^*)$ as a function of rotation. Repeating this process produces a series of such curves. The spread in values of $f(nm_e^*+pm_h^*)$ obtained for a specific angle is a measure of the error in the mass density introduced by experimental probe misalignment.

There are six combinations of microwave electric field and external magnetic field parallel to principal crystal axes. The microwave field was always perpendicular to the magnetic field. Two or more samples of differing shape and thickness were studied for each orientation. Samples as thick as 8.60 mm gave the same results for mass density as a sample 2.00 mm thick. No effect due to sample shape was found.

Samples were placed in the experimental probe with one crystal axis aligned with a mark on the probe. The final alignment was determined using extrema in the data for some samples. Samples with the trigonal and bisectrix axis perpendicular to the surface could be oriented on the extrema of the data.

The samples with the binary direction perpendicular to the surface could not be directly oriented on the extrema of the data. When the magnetic field and microwave electric field are in the trigonal-bisectrix plane the data shows a very broad minimum in $f(nm_e^*+pm_h^*)$ versus rotation angle near the bisectrix direction as shown in Fig. 3. For the magnetic field near

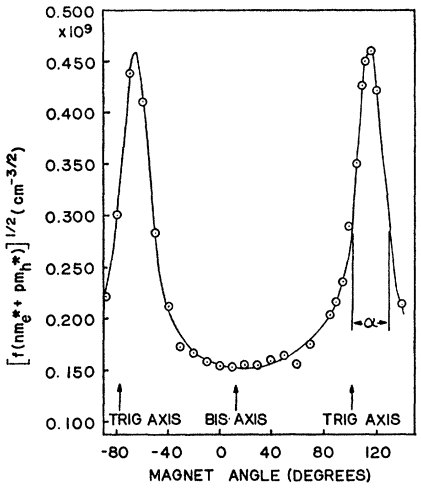

FIG. 3. Square root of the Alfvén-wave mass density plotted versus magnet orientation. The solid curve is a hand-drawn smooth curve through the data points. It is indistinguishable from the theoretical curve, as discussed in the text. α is the angular width of the peak at the trigonal axis value for the mass density. The angles are experimental angles for the magnet rotation and bear no relation to the location of any symmetry axis of the crystal.

the trigonal axis in this same sample there is a very sharp maximum which occurs off the principal axis as shown in Fig. 3. For the magnetic field parallel to the trigonal axis

$$f(nm_e^*+pm_h^*)=m_1[n_1+\tfrac{1}{4}(n_2+n_3)]+[m_2-(m_4^2/m_3)]\tfrac{3}{4}(n_2+n_3)+pM_1, \quad (16)$$

where n_1 is the number of electrons in ellipsoid 1, n_2 is the number in ellipsoid 2, n_3 is the number of electrons in ellipsoid 3, and p is the number of holes. The terms m_2 and m_4^2/m_3 are the largest terms in this expression and m_1 is the smallest. Therefore the expression for $f(nm_e^*+pm_h^*)$ is dominated by ellipsoids 2 and 3 for the magnetic field near the trigonal axis. Using a computer, it was possible to compute expected Alfvén-wave mass densities as the magnetic field varied from trigonal to bisectrix axes for various sets of mass parameters. We used the masses reported by Galt *et al.*,[24] Smith, Hebel, and Buchsbaum,[25] Kao,[26] Smith, Baraff, and Rowell,[27] and Brandt *et al.*[19] These values are listed in Table I. For each set of masses the angular difference between the calculated peak of the data in Fig. 3 and the trigonal axis is roughly twice the tilt angle. These numbers are tabulated in Table II. In the expression for the conductivity for each ellipsoid there is an angle-dependent denominator.[28] For electron ellipsoid 1 this denominator

[24] J. K. Galt, W. A. Yager, F. R. Merrit, B. B. Cetlin, and A. D. Brailsford, Phys. Rev. **114**, 1396 (1959).
[25] G. E. Smith, L. C. Hebel, and S. J. Buchsbaum, Phys. Rev. **129**, 154 (1963).
[26] Yi-Han Kao, Phys. Rev. **129**, 1122 (1963).
[27] G. E. Smith, G. A. Baraff, and J. M. Rowell, Phys. Rev. **135**, A1118 (1964).
[28] B. Lax, K. J. Button, H. J. Zeiger, and L. Roth, Phys. Rev. **102**, 715 (1956).

TABLE I. Electron and hole masses for bismuth reported in the literature and the values from this work.

	Electrons					Holes	
	m_1	m_2	m_3	m_4	m_4^2/m_3	$M_1=M_2$	M_3
Galt *et al.*[a]	0.0088	1.80	0.023	±0.16	1.113	0.068	0.92
SHB[b]	0.0062	1.30	0.017	−0.085	0.425	0.057	0.77
Kao[c]	0.0071	1.70	0.0301	0.177	1.041	0.0675	0.76
SBR[d]	0.00521	1.20	0.0204	−0.090	0.397	0.064	0.69
Brandt *et al.*[e]	0.00520	1.50	0.03	±0.16	0.855	0.066	0.62
This work	0.0050	1.27	0.031	±0.157	0.790	0.064	0.69

[a] Reference 24.
[b] Reference 25.
[c] Reference 26.
[d] Reference 27.
[e] Reference 19.

has a minimum at an angular value, θ, given by $\tan2\theta=2m_4/(m_2-m_3)$. The angle θ is the tilt angle of the electron Fermi surface ellipsoid. For ellipsoids 2 and 3 this denominator has a minima at an angular value, γ, given by

$$\tan2\gamma=-4m_4/(m_2+3m_1-4m_3). \quad (17)$$

Since m_3 and $3m_1-4m_3$ are small compared to m_2, we have $|\tan2\theta|\simeq-2m_4/m_2$ and $|\tan2\gamma|\simeq-4m_4/m_2$. For the range of mass values in Table I the angle γ is to a good approximation twice as large as the tilt angle θ in magnitude and of opposite sign. Since ellipsoid 2 and 3 dominate the behavior of $f(nm_e^*+pm_h^*)$ for magnetic fields near the trigonal axis, it would seem that the angle γ given by $\tan2\gamma=-4m_4/(m_2+3m_1-4m_3)$ is the angle between the trigonal axis and the peak of the data in Fig. 3. This result can be used to find the position of the principal crystal axis on a plot of mass density versus rotation angle.

Further justification for this method of orientation for these samples can be found in the de Haas–Shubnikov data of Bhargava.[18] In Fig. 3 of his paper the electron de Haas–Shubnikov periods are plotted as a function of rotation angle from trigonal to bisectrix axis. The upper curve has a maximum period of about 8.3×10^{-5} G^{-1} and a minimum period of about 0.7×10^{-5} G^{-1} with the minimum occurring off of the trigonal axis by the tilt angle θ, given by $\tan2\theta=2m_4/(m_2-m_3)$. This curve is associated with electron ellipsoid 1. The lower curve, associated with ellipsoids 2 and 3, has a maximum of about 4.3×10^{-5} G^{-1} and a minimum of about 0.7×10^{-5} G^{-1}. The minimum occurs off the trigonal axis by roughly twice the tilt angle in the opposite sense to the other minimum. Bhargava's curves are typical of the oscillation period versus rotation angle from any oscillatory experiments performed on bismuth.[29]

The transmitted microwave intensity amplitude in these experiments is modulated by the de Haas–Shubnikov oscillation.[9,15] This modulation is visible on the records, Fig. 2, and the periods of these oscillations versus angle are shown in Fig. 4. It must be noted that the values for the de Haas–Shubnikov periods near the minimum in Fig. 4 are due to holes. The maximum in Fig. 4 is due to electron periods. Using Bhargava's Fig. 3 to fit the points near the maximum in Fig. 4, we can determine the angle at which the electron-period minimum should occur. This angle is the same angle at which the maximum Alfvén-wave velocity occurs, Fig. 3. This procedure indicates experimentally that the Alfvén-wave velocity maximum in Fig. 3 is located off the trigonal axis by twice the tilt angle to the approximations used here. Bhargava gives a value for the tilt angle of 6.5°±0.25°. Table III shows other values of the tilt angle that have been reported. The recent determinations of the tilt angle indicate that 6.3° is a good compromise figure. This requires that the trigonal axis lies about 12.6° to the left of the peak in Fig. 3. The bisectrix axis then lies 90° from the trigonal axis. As is seen in the results, this procedure gives a consistent set of Alfvén mass densities.

IV. RESULTS

Table IV shows the results of this work and values from other Alfvén-wave experiments. In this table $[f(nm_e^*+pm_h^*)]^{1/2}$ is obtained directly from the experimental Alfvén-wave velocities. Table V uses these experimental numbers to calculate values of n, number of carriers, using the various sets of mass parameters in Table I.

TABLE II. $f(nm_e^*+pm_h^*)$ and $nm_4^2/2m_3$ calculated from the mass values of Table I, for both the trigonal direction and the maximum in the trigonal-bisectrix plane. A value for n of 3.0×10^{17} cm^{-3} is used. The angle of separation between the trigonal value and the peak value is compared with θ and γ as discussed in the text.

	$f(nm_e^*+pm_h^*)$ peak (10^{17} cm^{-3})	$f(nm_e^*+pm_h^*)$ trigonal (10^{17} cm^{-3})	Difference of columns 1 and 2 (10^{17} cm^{-3})	$nm_4^2/2m_3$ (10^{17} cm^{-3})	Angle between peak and trigonal axis	θ given by $\tan2\theta=2m_4/m_2-m_3$	γ given by $\tan2\gamma=-4m_4/m_2+3m_1-4m_4$
Galt *et al.*[a]	2.91[7]	1.24[8]	1.669	1.670	10.1°	5.1°	10.1°
Brandt *et al.*[b]	2.45[7]	1.17[6]	1.281	1.280	12.1°	6.05°	12.3°
SBR[c]	2.00°	1.40[4]	0.596	0.596	8.6°	4.35°	8.8°
SHB[d]	2.13°	1.49[3]	0.637	0.638	7.5°	3.77°	7.6°
Kao[e]	2.76[3]	1.20[2]	1.561	1.561	11.8°	5.9°	10.8°

[a] Reference 24.
[b] Reference 19.
[c] Reference 27.
[d] Reference 25.
[e] Reference 26.

[29] Tadao Fukuroi, Yoshio Muto, Yoshitami Saito, Kunihide Tanaka, and Tetsuo Fukase, Sci. Rept. Res. Inst. Tohoku Univ. Suppl. **A18**, 418 (1966).

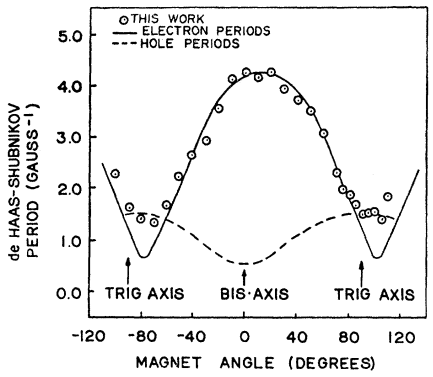

FIG. 4. The de Haas–Shubnikov periods for a sample of thickness 8.60 mm at experimental frequency 17.658 GHz and temperature 1.2°K. The solid curve is that of the electron periods and the dashed curve is that of the hole periods, both from Ref. 18.

TABLE III. Values of the tilt angle for bismuth as reported in the literature.

Investigator	Tilt angle (deg)
Galt *et al.*[a]	5.05
Boyle and Brailsford[b]	3.68
Jain and Koenig[c]	4.95
Weiner[d]	5.91
Kao[e]	5.98
SHB[f]	3.78
SBR[g]	4.33
Brandt *et al.*[h]	6.00
Eckstein and Ketterson[i]	4.00
Korolyuk[j]	6.1
Vol'skii[k]	6.0
Edel'man and Khaikin[l]	6.3
Bhargava[m]	6.5
Brown *et al.*[n]	6.0

[a] Reference 24.
[b] W. S. Boyle and A. D. Brailsford, Phys. Rev. **120**, 1943 (1966).
[c] A. L. Jain and S. H. Koenig, Phys. Rev. **127**, 442 (1962).
[d] D. Weiner, Phys. Rev. **125**, 1226 (1962).
[e] Reference 26.
[f] Reference 25.
[g] Reference 27.
[h] Reference 19.
[i] Y. Eckstein and J. B. Ketterson, Phys. Rev. **137**, A1777 (1965).
[j] Reference 21.
[k] E. P. Vol'skii, Zh. Eksperim. i Teor. Fiz. **46**, 2035 (1964) [English transl.: Soviet Phys.—JETP **19**, 1371 (1964)].
[l] Reference 20.
[m] Reference 18.
[n] R. D. Brown, R. L. Hartman, and S. H. Koenig, Phys. Rev. **172**, 598 (1968).

In Table V the first four lines give relatively consistent values for n. The masses of Galt *et al.* give consistent results for all six lines, but the values for the number of carriers appear to be low. Recent investigators, Table VI, arrive at values for n between 2.8×10^{17} cm^{-3} and 3.1×10^{17} cm^{-3}. In the data in Table IV, the greatest discrepancy between different observers occurs for lines 5 and 6. This discrepancy results from the difficulty of aligning the magnetic field accurately along the trigonal axis, and the extreme sensitivity to minor misalignments.

As an example of this sensitivity to alignment, Fig. 5 shows experimental mass density data in the trigonal-binary plane. The sample is a bisectrix sample (bisectrix axis perpendicular to the surface). The three data plots in Fig. 5 arise from misalignments which are rotations about the binary axis, that is, rotations which move the bisectrix toward the trigonal axis. After the sample was misaligned in this manner, a full rotation pattern of Alfvén-wave velocities was measured. The three plots show an extreme sensitivity to alignment near the trigonal axis. Figure 6 is a plot of data taken with the magnetic field nominally along the trigonal axis but misaligned varying amounts in the trigonal-bisectrix plane. Misalignment of the sample by $\pm1°$ in this plane can be seen to cause a spread of experimental values for $f(nm_e^*+pm_h^*)$ between 0.285×10^9 cm$^{-3/2}$ and 0.327×10^9 cm$^{-3/2}$. This particular orientation corresponds to the data in line 5, Table IV.

As discussed in Sec. III, the amount of sample misalignment can be checked by rotating the sample with respect to the sample holder. For a bisectrix sample the variation in the experimental value for line 5 using this technique was from 0.285×10^9 cm$^{-3/2}$ to 0.310×10^9 cm$^{-3/2}$. Using Fig. 6, this corresponds to an error in alignment of 1°. This agrees with the accuracy expected from the precision of the x-ray and mechanical alignment of the samples.

The data of line 6 correspond to the magnetic field in the trigonal-bisectrix plane of a binary sample (binary axis perpendicular to the surface). Since the extremum in the data, Fig. 3, is *not* along a principal crystal axis, alignment is difficult. The trigonal axis was shown in Sec. III to be *twice* the tilt angle away from the extremum in the data. Using values for the tilt angle from 6° to 6.5° indicates that the trigonal axis is between 12°

TABLE IV. $[f(nm_e^*+pm_h^*)]^{1/2}$ obtained by various workers, in units of 10^9 cm$^{-3/2}$.

$B\|\|$ axis	$E\|\|$ axis	Present work	McLachlan[a]	Williams[b]	Faughnan[c]	Kirsch[d]	Khaikin[e]	Faughnan[c]
1	2	0.470	0.429	0.481	0.464	0.548	0.515	0.718
1	3	0.380	0.363	0.318	0.406	0.378	0.407	0.322
2	1	0.460	0.461	0.470	0.700		0.467	0.602
2	3	0.155	0.146	0.162	0.140	0.153	0.156	0.171
3	1	0.300	0.315	0.393	0.362			0.322
3	2	0.310	0.304	0.460	0.478	0.312		0.400

[a] Reference 9.
[b] Reference 7.
[c] Reference 10.
[d] Reference 4 using $n=3\times10^{17}$ cm^{-3}.
[e] Reference 6 using $n=3\times10^{17}$ cm^{-3} and correcting for a factor of 2 as noted in M. S. Khaikin and V. S. Edel'man, Zh. Eksperim. i Teor. Fiz. **49**, 1695 (1966) [English transl.: Soviet Phys.—JETP **22**, 1159 (1966)].

TABLE V. Experimental mass densities, expressions for $f(nm_e^*+pm_h^*)$ from the conductivity tensor, and values of n calculated from these data for the mass values of Table I.

$H\|\|$ axis	$E\|\|$ axis	$f(nm_e^*+pm_h^*)$ (10^{17} cm^{-3})	$f(nm_e^*+pm_h^*)$	n(calculated) Galt *et al.*[a]	SHB[b]	Kao[c]	SBR[d]	Brandt *et al.*[e]	This work
				(all values below are $\times 10^{17}$ cm^{-3})					
1	2	2.22	$n\left(m_3-\frac{2m_4^2}{m_1+3m_2}+M_3\right)$	2.1[8]	2.7[2]	2.7[2]	3.0[2]	3.3[2]	3.1[8]
1	3	1.44	$n\left(\frac{m_2}{3}+\frac{8m_1m_2}{3(m_1+3m_2)}+M_2\right)$	2.1[3]	2.9[0]	2.2[4]	3.0[5]	2.5[2]	3.0[7]
2	1	2.12	$n\left(m_3-\frac{m_4^2}{3m_2}-\frac{2m_4^2}{3(3m_1+m_2)}+M_3\right)$	2.2[7]	2.8[4]	2.8[4]	3.1[5]	3.4[4]	3.0[2]
2	3	0.241	$n\left(\frac{m_1}{3}+\frac{8}{3}\frac{m_1m_2}{3m_1+m_2}+M_1\right)$	2.5[5]	3.2[0]	2.7[1]	3.0[2]	2.9[6]	3.0[2]
3	1	0.900	$\frac{1}{2}n\left(m_1+m_2-\frac{m_4^2}{m_3}+2M_2\right)$	2.1[8]	1.8[0]	2.2[5]	1.9[2]	2.6[5]	3.0[2]
3	2	0.930	$\frac{1}{2}n\left(m_1+m_2-\frac{m_4^2}{m_3}+2M_1\right)$	2.1[6]	1.8[6]	2.3[2]	1.9[2]	2.6[5]	3.0[2]

[a] Reference 24.
[b] Reference 25.
[c] Reference 26.
[d] Reference 27.
[e] Reference 19.

and 13° from the peak of the data in Fig. 3. This gives a spread of $[f(nm_e^*+pm_h^*)]^{1/2}$ on the trigonal axis from 0.310×10^9 cm$^{-3/2}$ to 0.305×10^9 cm$^{-3/2}$.

Looking at the $[f(nm_e^*+pm_h^*)]^{1/2}$ values reported by the first three investigators in Table IV, we find that most of the discrepancy among their results can be explained in terms of an angular alignment difference of 3° or less. Another factor contributing to different $[f(nm_e^*+pm_h^*)]^{1/2}$ values is the quantum oscillation of mass densities as reported by Williams and Smith.[8] These oscillations will be discussed further in a future paper. The values of $[f(nm_e^*+pm_h^*)]^{1/2}$ are determined by a least-squares fit of a straight line to the N versus $1/H$ curves. If the magnetic field range investigated extends only from the peak of one oscillation to the trough of another, then the reported value of $[f(nm_e^*+pm_h^*)]^{1/2}$ will be high or low. This is most evident in the trigonal samples. From this discussion it appears than an alignment accuracy of $\pm1°$ is not really sufficient for Alfvén-wave measurements on the Fermi surface of bismuth with the magnetic field along the trigonal axis.

TABLE VI. Values for the number of carriers in bismuth as reported in the recent literature.

Investigator	Number of electrons (10^{17} cm^{-3})	Number of holes (10^{17} cm^{-3})
McCombe and Seidel[a]		2.88
Bhargava[b]	2.88	3.00
Brandt and Lyubutina[c]	2.8	2.8
Korolyuk[d]	2.76	
Brandt *et al.*[e]	3.0	2.76
SBR[f]	2.75	2.75
Williams[g]	3.1	3.1

[a] B. McCombe and G. Seidel, Phys. Rev. **155**, 633 (1967).
[b] Reference 18.
[c] N. B. Brandt and L. G. Lyubutina, Zh. Eksperim. i Teor. Fiz. **47**, 1711 (1965) [English transl.: Soviet Phys.—JETP **20**, 1150 (1965)].
[d] Reference 21.
[e] Reference 19.
[f] Reference 27.
[g] Reference 7.

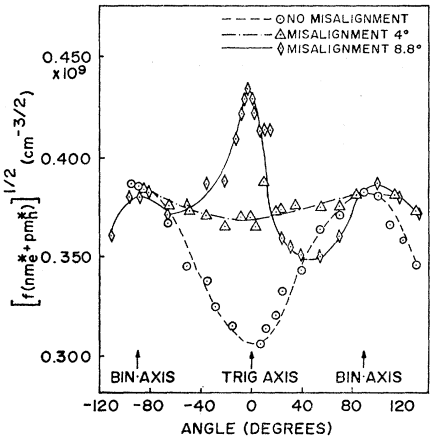

FIG. 5. Square root of the Alfvén-wave mass density for various misalignments of the crystal. The sample is tilted around the binary axis displacing the trigonal axis toward the bisectrix axis.

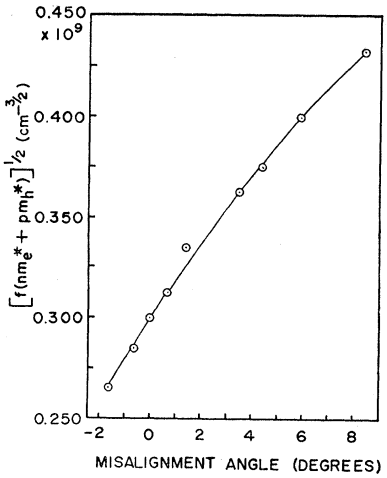

FIG. 6. Square root of the Alfvén-wave mass density versus sample misalignment. This shows in more detail the variation in mass density as the sample is tilted around the binary axis. The misalignment angle corresponds to the angle the magnetic field is tilted away from the crystal trigonal axis in the trigonal-bisectrix crystal plane.

V. DISCUSSION

The Alfvén-wave experiments produce six principal axis results for $f(nm_e^*+pm_h^*)$. The experimental values, given in Table IV, are obtained using the alignment procedures discussed in Sec. III. There are seven unknowns among these expressions for the Alfvén-wave mass densities, as seen in Table V. It is generally agreed that the hole masses M_1 and M_2 are equal. Assuming this to be true, there are six equations in six unknowns. It should be possible to determine the number of carriers n, the electron masses, and the hole mass M_3 from these equations. In practice this is not feasible since some of the electron masses are small compared to the others. It is possible with the aid of outside information to estimate values of the mass parameters. Three different methods of doing this are presented below.

A. Since, in the reported mass values in Table I, $m_1 \ll m_2$, it is convenient to anticipate this result and use it to simplify the expressions for $f(nm_e^*+pm_h^*)$ appearing in Table V. The resulting expressions are

$$n[m_3-(2m_4^2/3m_2)+M_3]=2.22\times10^{17}\ \text{cm}^{-2}, \quad (18)$$

$$n[\tfrac{1}{3}(m_2)+M_2]=1.44\times10^{17}\ \text{cm}^{-3}, \quad (19)$$

$$n[m_3-(m_4^2/m_2)+M_3]=2.12\times10^{17}\ \text{cm}^{-3}, \quad (20)$$

$$n[3m_1+M_1]=0.241\times10^{17}\ \text{cm}^{-3}, \quad (21)$$

$$n[\tfrac{1}{2}(m_2)-(m_4^2/2m_3)+M_2]=0.900\times10^{17}\ \text{cm}^{-3}, \quad (22)$$

$$n[\tfrac{1}{2}(m_2)-(m_4^2/2m_3)+M_2]=0.930\times10^{17}\ \text{cm}^{-3}, \quad (23)$$

where the numerical values are the experimental results of this work.

TABLE VII. Experimental values of the hole masses as reported in the literature.

Investigator	M_1M_3	M_1M_2	$M_1=M_2$	M_3
Galt *et al.*[a]	0.0625	0.00462	0.068	0.920
SHB[b]	0.0441	0.00326	0.057	0.770
SBR[c]	0.0441	0.00410	0.064	0.690
Kao[d]	0.0513	0.00465	0.0675	0.760
Grenier *et al.*[e]	0.0556	0.00423	0.0650	0.855
Edel'man and Khaikin[f]	0.0412	0.00397	0.063	0.655
Edel'man and Khaikin[f]	0.0441	0.00410	0.064	0.690
Swada[g]	0.0400	0.00372	0.061	0.655
McCombe and Seidel[h]	0.0441	0.00410	0.064	0.690
Brandt[i]	0.0436	0.00435	0.066	0.620

[a] Reference 24.
[b] Reference 25.
[c] Reference 27.
[d] Reference 26.
[e] C. G. Grenier, M. M. Reynold, and J. R. Sybert, Phys. Rev. **132**, 58 (1963).
[f] Reference 20.
[g] Y. Swada, J. Phys. Soc. Japan Suppl. **21**, 760 (1966).
[h] B. McCombe and G. Seidel, Phys. Rev. **155**, 633 (1967).
[i] Reference 19.

The hole-cyclotron masses $(M_1M_2)^{1/2}$ and $(M_1M_3)^{1/2}$, as measured by de Haas–van Alphen, de Haas–Shubnikov, and cyclotron resonance experiments, appear to be the best-known masses for bismuth. Table VII shows the values of M_1M_3 and M_1M_2 as measured by several investigators. The value most often found for M_1M_3 is 0.0441. If we assume $M_1=M_2$ and use the average of the values found for M_1M_2 of 0.00411, this gives $M_1=M_2=0.064$. In turn this gives a value for $M_3=0.69$. From the reported values of electron masses $m_3-2m_4^2/3m_2$ and $m_3-m_4^2/m_2$ are about 2–3% of M_3. If we replace Eqs. (18) and (20) by $nM_3=2.17\times10^{17}$ cm^{-3}, we can solve for n. If we then lower the answer by 3%, we obtain a value for n which includes the two small terms. We then use Eq. (19) to find m_2, Eq. (21) to find m_1, and Eq. (22) or (23) to find $m_4^2/2m_3$. The results of this approach are

$$n=3.07\times10^{15}\ \text{cm}^{-3},$$
$$m_1=0.005,$$
$$m_2=1.21,$$
$$m_4^2/2m_3=0.76,$$
$$M_1=0.064,$$
$$M_3=0.69.$$

B. We may also estimate the mass parameters by the procedure used by Williams.[7] Replace Eqs. (18) and (20) by $nM_3=2.17\times10^{17}$ cm^{-3}. As discussed, this figure is high by about 3%; consequently we will reduce it by this amount, and use $nM_3=2.10\times10^{17}$ cm^{-3}. We also assume $M_1M_3=0.0441$. Equation (21) gives $n(3m_1+M_1)=0.241\times10^{17}$. If we assume values for m_1 obtained from the various reported values, then we can solve Eqs. (18), (20), and (21) simultaneously for n, M_3, and M_1. We can then use Eqs. (19) and (22) or (23) to find m_2 and m_4^2/m_3, with m_1 being obtained from values in Table I.

The results for this procedure are

$$n=(2.99\pm0.16)\times10^{17}\ \text{cm}^{-3},$$
$$m_1=0.0055\pm0.0015,$$
$$m_2=1.26\pm0.07,$$
$$m_4^2/m_3=0.790\pm0.05,$$
$$M_1=0.0625\pm0.0015,$$
$$M_3=0.707\pm0.017,$$

where the $\pm$ deviations correspond to the $\pm$ variations in the values of m_1 used.

C. A third approach depends on the properties of the ellipsoidal Fermi surface model. From Table II, we note that, using the mass values of Table I, the difference between the maximum value of $f(nm_e^*+pm_h^*)$ and the value of $f(nm_e^*+pm_h^*)$ on the trigonal axis is equal to $(n/2)(m_4^2/m_3)$. The peak value for $f(nm_e^*+pm_h^*)$ from Fig. 3 is 2.11×10^{17} cm^{-3}; the trigonal axis value is 0.900×10^{17} cm^{-3} or 0.930×10^{17} cm^{-3}. We can then substitute for Eqs. (22) and (23)

$$nm_4^2/2m_3=1.21\times10^{17}\quad\text{or}\quad1.18\times10^{17}\ \text{cm}^{-3},\quad(24)$$
$$n[\tfrac{1}{2}(m_2)+M_2]=2.11\times10^{17}\ \text{cm}^{-3}.\quad(25)$$

Using Eq. (21) with $M_1=0.064$ and reported values for m_1, we can estimate n. From Eq. (25) with $M_1=M_2$, we can evaluate m_2, and from Eq. (24) we obtain m_4^2/m_3. Using $nM_3=2.10\times10^{17}$ cm^{-3}, we can obtain M_3. The results are

$$n=(3.01\pm0.16)\times10^{17}\ \text{cm}^{-3},$$
$$m_1=0.0055\pm0.0015,$$
$$m_2=1.22\pm0.04,$$
$$m_4^2/m_3=0.790\pm0.050,$$
$$M_1=0.064,$$
$$M_3=0.702\pm0.04.$$

It is possible to estimate m_4 from the shape of the data curve in Fig. 3. The peak of the Alfvén-wave mass density in Fig. 3 is symmetrical. The angular separation between the peak and the trigonal axis is nearly twice the tilt angle, as discussed in Sec. III and summarized in Table II. Therefore, the width of the peak in Fig. 3 at $f(nm_e^*+pm_h^*)$ equal to its experimental value should be nearly four times the tilt angle. The tilt angle, θ, is given by $\tan2\theta=2m_4/(m_2-m_3)$. If we call the angular width of the peak at the trigonal axis value α, shown in Fig. 3, then $\alpha=4\theta$. The angular width α is related to the mass parameters by

$$|\tan\tfrac{1}{2}\alpha|=2m_4/m_2.\quad(26)$$

We have neglected terms like m_3/m_2 since they are small compared to the other terms.

From line 5 of Table IV we have $[f(nm_e^*+pm_h^*)]^{1/2}$ equal to 0.300×10^9 cm$^{-3/2}$. This is directly measured from the minimum in the rotation patterns as discussed in Sec. III. By drawing a smooth curve through the experimental points, Fig. 3, the angular width α turns out to be 28°. The value of $f(nm_e^*+pm_h^*)$ from line 6 of Table IV is 0.310×10^{17} cm^{-3}. This was obtained by assuming a tilt angle, θ, of 6.5°. This means that α should be 26°. In this section we developed a value for m_2 which is 1.27 ± 0.07. Using this value of m_2 in Eq. (26), we obtain m_4 equal to 0.157 ± 0.008. We have also found that m_4^2/m_3 is 0.790 ± 0.050. Combining this last result with the value for m_4, we obtain m_3 equal to 0.028 ± 0.04.

As a check of consistency, the masses developed in this section were used to fit the trigonal-bisectrix curve. The Alfvén-wave experiments are most sensitive to the heavy masses, m_2, m_4^2/m_3, M_3, and the number of carriers, n. The trigonal-bisectrix curve depends on the largest number of these parameters. A good fit would obviously fit both the maximum and the minimum, and would also fit the width of the peak since this depends on m_4. The theoretical fit was obtained with the following values for the mass parameters (the best-fit theoretical curve is indistinguishable from the hand-drawn smooth curve in Fig. 3):

$$m_1=0.005\pm0.0015,$$
$$m_2=1.27\pm0.07,$$
$$m_3=0.031\pm0.004,$$
$$m_4=\pm0.157\pm0.008,\quad(27)$$
$$M_1=0.064,$$
$$M_3=0.069,$$
$$n=(3.00\pm0.15)\times10^{17}\ \text{cm}^{-3}.$$

Using the parameters in Eq. (27), we calculate $[f(nm_e^*+pm_h^*)]^{1/2}$ to compare with the experimental values in this work. This comparison is shown in the last column of Table V. The agreement with a value of $n=3.0\times10^{17}$ cm^{-3} is good, which indicates the set of parameters shown in Eq. (27) is consistent.

In summary, we have measured the Alfvén-wave mass densities in bismuth. No dependence on sample shape or thickness was found. The variation of Alfvén-wave mass densities previously reported in the literature can be interpreted as a difference in sample alignment among the various investigators. We have used the experimental Alfvén-wave mass densities to compute a consistent set, Eq. (27), of carrier masses and the number of carriers. The masses measured are the transport masses at the Fermi surface. The de Haas–Shubinkov periods in bismuth have been measured from the envelope of the transmitted microwave signal.

ACKNOWLEDGMENTS

We wish to thank Dr. Earl H. Hygh, Peter Temple, and Franz Rosenberger for helpful discussions and technical assistance during this work, and Dr. Seymour Koenig for a critical reading of the manuscript.